Plasmonics (2022) 17:1973–1984
https://doi.org/10.1007/s11468-022-01685-w

Sensitivity-Enhanced Surface Plasmon Resonance Sensor with Bimetal/ Tungsten Disulfide (WS_2)/MXene ($Ti_3C_2T_x$) Hybrid Structure

Maryam Ghodrati[1] · Ali Mir[1] · Ali Farmani[1]

Received: 29 April 2022 / Accepted: 14 June 2022 / Published online: 25 June 2022

Abstract

This work aims at improving the sensitivity of a surface plasmon resonance (SPR) sensor with the BK7 prism, silver/gold (Ag/Au) bimetallic films, 2D materials tungsten disulfide (WS_2), and MXene ($Ti_3C_2T_x$) under angular interrogation technique. The proposed SPR sensor is a free space structure using the Kretschmann configuration to stimulate surface plasmons (SPs). The finite-difference time-domain (FDTD) method is used to analyze the optical behavior of the proposed SPR sensor. The thickness of the bimetallic layers and the number of layers of 2D materials are optimized to obtain maximum sensitivity for various sensing medium refractive indices ranging from 1.33 to 1.335 RIU. The maximum sensitivity of 348 deg/RIU is obtained with a thickness of 33 nm Ag, a thickness of 15 nm Au and with monolayer WS_2, and four layers of $Ti_3C_2T_x$ MXene at 633 nm. This excellent performance of the proposed structure makes it suitable for detecting biomolecules and other analytes.

Keywords 2D material · Sensitivity · Surface plasmon resonance · $Ti_3C_2T_x$ MXene · Sensor

Introduction

The surface plasmon resonance phenomenon is the resonant coupling of electromagnetic waves to the charge density oscillations at the interface of dielectrics and metals [1–3]. Due to the mismatch of optical momentum between the SPR mode and light in free space, the optical excitations in the SPR occur with the attenuated total reflection (ATR) method, which was proposed by Kretschmann [2] and Otto [3]. There is only a TM-polarized electric field for surface plasmon waves (SPWs). These waves are exponentially decayed at the interface between the dielectric and the metal [1, 3–6]. SPR sensors have potential advantages such as real-time and label-free detections, quick response, high sensitivity, cost-effectiveness, high-resolution detection, etc., which has led to their diverse applications [7–9]. Various applications of SPR sensors include environment monitoring, medical diagnostics such as detection of human blood group, DNA, glucose, virus, living cell analysis, and gas sensing [10–13]. In general, noble metals such as gold (Au), silver (Ag), aluminum (Al), and copper (Cu) are widely used plasmonic materials for SPR sensors [5, 6, 14–16]. Gold and silver are mostly used in SPR sensors because of their excellent chemical stability, better biological affinity, higher sensitivity, and a great figure of merit in comparison to other metals [5, 6, 17–19]. The SPR sensor based on Au shows a broader full width at half maximum (FWHM) that reduces the accuracy of analyte detection while the SPR sensor based on Ag displays higher detection accuracy and lower sensitivity in comparison to Au metal. A bimetallic film of Ag-Au combines the advantages of both of them, representing its superior candidature for SPR sensors [20–22]. The 2D materials have desirable physical and structural properties and are well-suited for applications in sensing and biosensing. This is due to great surface adsorption, direct bandgap, and unique optical, chemical, thermal, magnetic, and electrical properties [23–25]. Transition-metal carbides and nitrides, known as MXenes, are 2D materials by the general formula $M_{n+1}X_nT_x$, where M represents an early transition metal, X is carbon and/or nitrogen, and T_x is the surface termination groups ((–O), (–F), and (–OH)) [7, 8, 26–28]. The n index indicates a variable number between 1 and 3. Among

✉ Ali Mir
mir.a@lu.ac.ir

[1] Faculty of Engineering, Lorestan University, Khoram-Abad, Iran

the types of MXene, $Ti_3C_2T_X$ MXene has shown potential in numerous fields, and due to its unique optical and electrical properties improves sensor performance and quality [8, 29–31]. Transition metal dichalcogenides (TMDs) are a class of 2D materials with the formula MX_2, where M stands for metal (Molybdenum or Tungsten) and X refers to chalcogenide (sulfur, selenium, or tellurium) like MoS_2, $MoSe_2$, WS_2, and WSe_2 offers tunable optical and electronic properties [30–32]. In recent years, the various structures of SPR sensors have been studied to improve the performance parameters of sensors, especially sensitivity. Vibisha et al. investigated the use of the TMDCs material over a Cu-Ni bimetallic layer to achieve the higher sensitivity with optimized Cu and Ni layer [5]. Zhao et al. reported the sensor structure using seven layers of WS_2 over Al metal and BK7 prism; the proposed sensor obtained a sensitivity of 315.5 deg/RIU [29]. Kumar et al. introduced the SPR sensor with Ag-Si-MXene and Ag-Si-BP-MXene to achieve high sensitivity of 231 deg/RIU and 264 deg/RIU, respectively [30, 31]. Yue et al. [32] proposed a SPR sensor consists of Ag-Au bimetallic structure with BlueP/TMDCs and graphene; the results showed that the sensitivity could be significantly increased. Shushama et al. presented an SPR sensor structure consisting of a hybrid structure with a silicon layer, a monolayer of MoS_2, and graphene on a BK7 prism; the offered structure improved sensitivity to around 210 deg/RIU [33]. The Kretschmann configuration is generally documented as one of the most basic SPR configurations for biosensors, and SPR with a single prism is a frequently utilized technique in sensor application. As mentioned earlier, 2D nanomaterials and their heterostructures like MXenes have extraordinary properties such as high surface-to-volume ratio, excellent electric conductivity, and high absorption; also, their surface can be functionalized with various analytes or nanobiomolecules. All these factors make them a suitable platforms for sensor and biosensor development. On the other hand, due to the rising steadily of human disease, we need easy-to-use and detectable sensing systems. Therefore, the development of reliable biosensor systems for multi-analytic detection is another need to be considered. In this regard, we presented a SPR sensor based on the BK7 prism, silver/gold (Ag/Au) bimetallic films, 2D materials tungsten disulfide (WS_2), and MXene ($Ti_3C_2T_x$) under angular interrogation technique. The proposed sensor is a free space structure using the Kretschmann configuration to stimulate SPs. There are too many papers reported in the literature which uses the 2D materials for the sensitivity enhancement but based on the knowledge of the authors, the heterostructure proposed based on Ag/Au bimetallic and WS_2-MXene composites here has not been used before. The novelty of the current paper lies in the use of Ag/Au bimetallic and WS_2-MXene ($Ti_3C_2T_x$) hybrid structure can effectively detect biomolecules at room temperature. In this paper, the minimum reflection (R_{min}), sensitivity, figure of merit (FOM), and detection accuracy (DA) of the SPR curve are investigated using the numerical method of FDTD in the visible regime. The results show by optimizing thickness of the bimetallic and the number of layers of 2D materials; the maximum sensitivity was achieved at 633 nm.

Materials and Sensor Design

The schematic of the proposed SPR sensor based on the Kretschmann structure is illustrated in Fig. 1a. The structure consists of six layers, including BK7 prism, Ag/Au bimetallic films, tungsten disulfide (WS_2), MXene ($Ti_3C_2T_x$), and sensing medium (SM).

The finite-difference time-domain (FDTD) technique is used to evaluate electromagnetic field analysis for the proposed sensor, which is a powerful method to solve Maxwell's equations in a nanofilm layer by using the YEE-algorithms [17, 20, 25]. In fact, a two-dimensional FDTD simulation is used for this analysis. The XY view of the FDTD simulation schematic for the proposed SPR biosensor is depicted in Fig. 1b. The parameter sweep is used for angular interrogation over a wide range of source angels (40 to 85°), in order to obtain the source angle capable to excite the SPR mode. The optical parameter was set as a plane-wave source (Bloch/periodic type) at an optical wavelength of 633 nm. The perfectly matched layer (PML) boundary condition was used in such a way that waves enter into the layers with generating minimum reflections. Also, for excitation of the SPW, the incident light is a transverse magnetic (TM) polarized. In proposed structure, we use BK7 prism with $n_{BK7} = 1.5151$ at $\lambda = 633$ nm as the coupling prism for exciting SPR. The refractive index (RI) of BK7 can be calculated from Eq. (1) [4, 29, 31] :

$$n_{BK_7}(\lambda) = \sqrt{\frac{1.03961212\lambda^2}{\lambda^2 - 0.00600069867} + \frac{0.231792344\lambda^2}{\lambda^2 - 0.0200179144} + \frac{1.01046945\lambda^2}{\lambda^2 - 103.560653} + 1} \quad (1)$$

In Eq. (1), λ represents the wavelength of incident light in μm scale. According to the Drude–Lorentz model, the refractive indexes of the metals are determined by [29–32] :

$$n_m(\lambda) = \sqrt{\left(\varepsilon'_m + i\varepsilon''_m\right)} = \sqrt{\left[1 - \frac{\lambda^2 \lambda_C}{\lambda_P^2\left(\lambda_C + i\lambda\right)}\right]} \quad (2)$$

where λ_p and λ_c represent the plasma and collision wavelength. The values of λ_p and λ_c for Ag are equal to 1.4541×10^{-7} m and 17.614×10^{-6} m, respectively [29–32], and the thickness of the Ag layer is 33 nm. To reduce the oxidation of the Ag layer, the Au film is deposited on the Ag layer. Furthermore, the use of a bimetallic structure

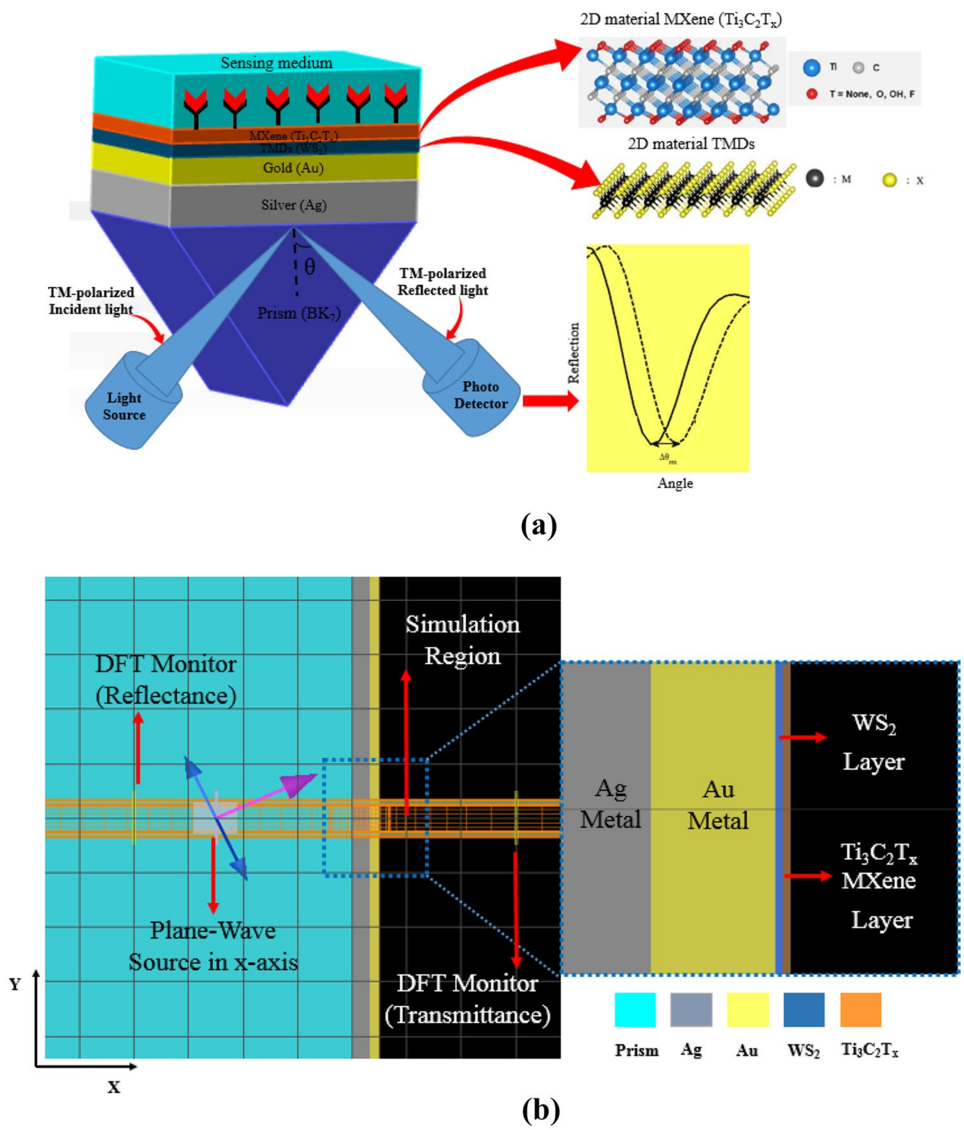

Fig. 1 **a** Schematic diagram of the proposed SPR sensor **b** XY view of the FDTD simulation schematic for the proposed SPR biosensor

enhances sensitivity in the SPR sensor highly. The values of λ_p and λ_c for Au are equal to 1.6826×10^{-7} m and 8.9342×10^{-6} m, respectively [29–32], and the thickness of the Au layer is 15 nm. We have chosen Ag/Au bimetallic films instead of single plasmonic metal. To stabilize the device, monolayer WS_2 was placed on the metal so that metal can free from the chemical reaction and a huge amount of light energy can be absorbed. The complex RI of tungsten disulfide (WS_2) is $n_{WS2}=4.89+0.314i$, and its thickness is equal to $d_{\mathrm{WS2}}=L\times0.8$ nm, where L is the number of WS_2 layers, and 0.8 is the thickness of a monolayer [29, 32]. $Ti_3C_2T_x$ MXene is deposited over WS_2 as a biorecognition element (BRE) layer for analytes due to its hydrophilic nature and large surface area. The complex RI of $Ti_3C_2T_x$ MXene is $n_{Mxene}=2.38+1.33i$, and its thickness is equal to $d_{\mathrm{MXene}}=L\times0.993$ nm, where L is the number of $Ti_3C_2T_x$ MXene layers and 0.993 is the thickness of a monolayer [4, 7]. Finally, the last layer is the sensing medium and the RI of this medium is given as $n_s=1.33+\Delta n_s$, where Δn_s is the change of RI in sensing medium due to the occurrence of a biological action. We have considered the sensing medium as an aqueous solution with a refractive index of 1.33 RIU and selected the refractive index changes with steps of 0.005 RIU. The adsorption of the molecule on the sensor surface changes the concentration of the aqueous solution, which in turn changes the RI of the sensing medium. In other words, this varies from 1.33 to 1.35 RIU when analyte is adsorbed at the MXene surface. The large surface area of $Ti_3C_2T_x$ MXene due to its layered nature provides an increased contact area for the attachment of the molecule.

Performance Parameters of the SPR Sensor

The performance parameters defined for the proposed SPR sensor are sensitivity, full width at half maximum (FWHM), detection accuracy (DA), and figure of merit (FOM). The FDTD numerical method is used to obtain all the performance parameters. The sensitivity is defined as the ratio of SPR angle shift ($\Delta\theta_{SPR}$) to the changes in refractive index (Δn_s) in the sensing medium by the following equation [20, 30, 32] :

$$S = \frac{\Delta\theta_{SPP}}{\Delta n_s} \quad (3)$$

The unit of sensitivity is expressed as deg/RIU. To better understand the sensing performance of the SPR sensors, another intelligent scale of measurement called FOM dimensioned at RIU^{-1} is used that is obtained from the ratio of the sensitivity to the FWHM based on Eq. (4) [20, 30, 32] :

$$FOM = \frac{S}{FWHM} \quad (4)$$

where FWHM is a difference of the resonance angles at 50% reflection intensity [29, 32]. FWHM also shows the angular width of the reflectance curve. Another critical parameter of the SPR sensor is the detection accuracy, dimensioned at deg^{-1}, and can be determined by taking the inverse of the FWHM of the SPR curve, using the following equation [29, 30, 32] :

$$DA = \frac{1}{FWHM} \quad (5)$$

Results and Discussion

First of all, we calculated the absorption spectrum of the conventional sensor structure by the numerical simulation and compared it with analytical results of transfer-matrix method (TMM), and the experimental Johnson-Christy model to prove the accuracy of our model. As shown in Fig. 2, there is a good agreement between the FDTD simulation with analytical results, and the experimental Johnson-Christy model, which confirms the validity and accuracy of our model. It is clear that the absorption peaks are close to each other. It should be noted that we have only done theoretical research but it is possible to implement it practically.

Here, we have considered different thicknesses of Ag and Au to determine the optimized thickness of bimetals. According to the literature, the metal layer plays a significant role in the generation of surface plasmons so the thickness optimization of Ag/Au metals is essential to balance the photon absorption efficiency as well as energy loss. Also, the use of bimetallic Ag/Au layers and 2D materials such as

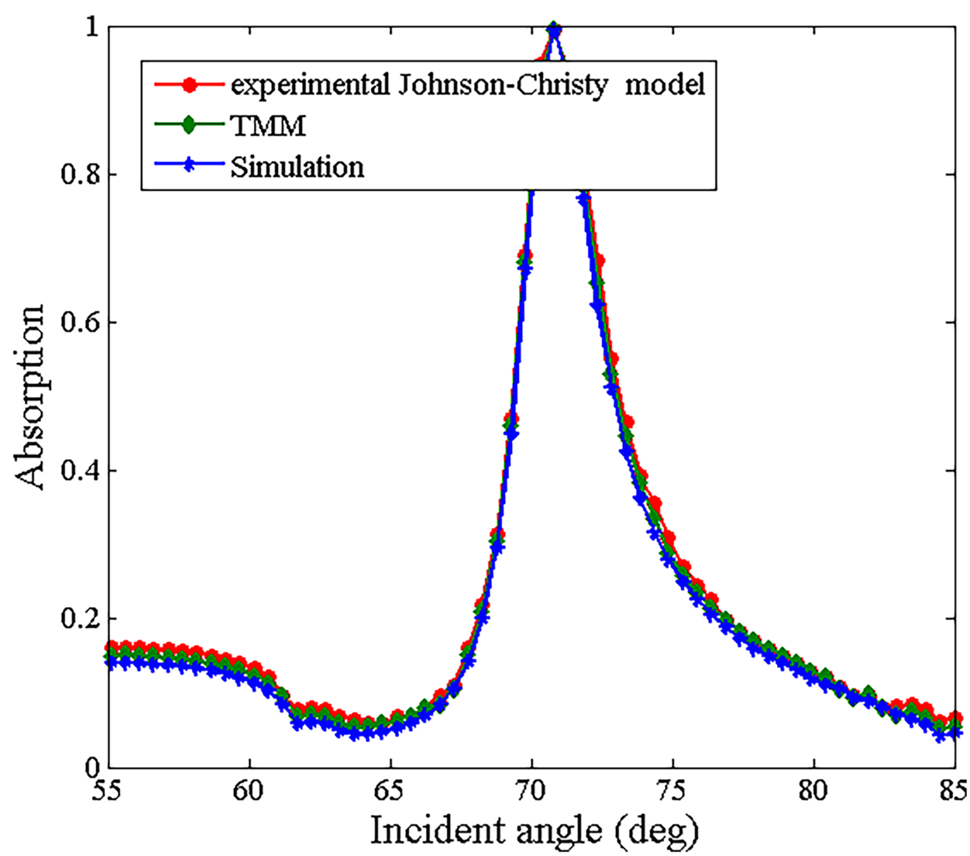

Fig. 2 The absorption spectrum of the conventional sensor structure and excellent agreement between the numerical simulation, the experimental Johnson-Christy model, and the analytical TMM results

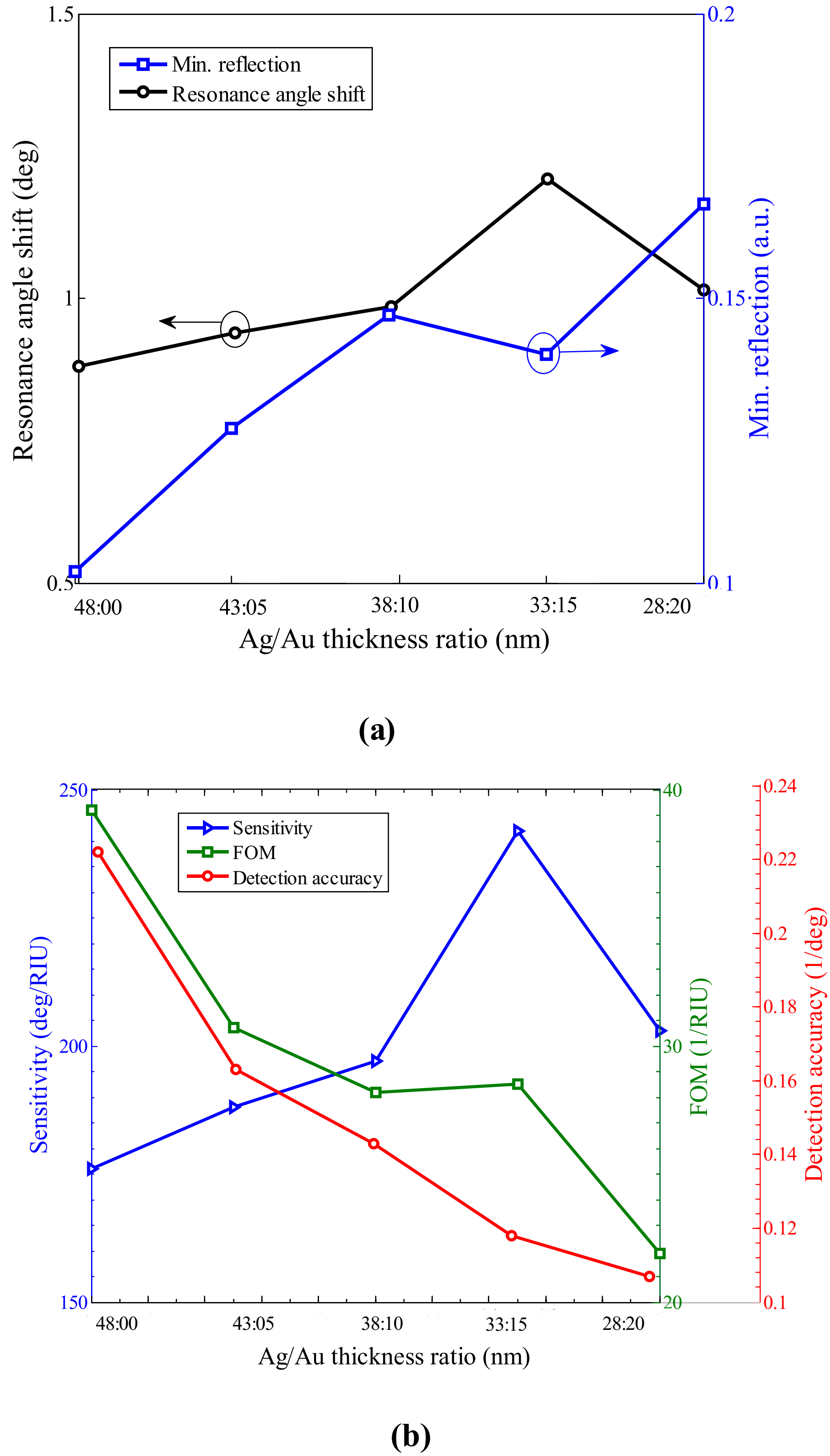

Fig. 3 Variation in **a** resonance angle shift and minimum reflection **b** sensitivity, detection accuracy, and FOM versus the Ag/Au thickness of the proposed SPR sensor

WS_2 and $Ti_3C_2T_x$ MXene over bimetallic Ag/Au layers in the proposed SPR sensor can contribute to sensitivity enhancement. We considered the thickness of the Ag layer equal to 28, 33, 38, 43, and 48 nm, and the Au layer thickness equal to 0, 5, 10, 15, and 20 nm, respectively. Figure 3a and b show resonance angle shift, minimum reflection, sensitivity, DA, and FOM in terms of Ag/Au thicknesses for the proposed SPR sensor. From Fig. 3a, the variation in resonance angle shift is obtained 0.88, 0.94, 0.985, 1.21, and 1.015 deg and the minimum reflection is calculated 0.1019, 0.1272, 0.1471, 0.1402, and 0.1666 a.u. for different thickness combinations of Ag and Au.

It is observed that the minimum reflection less than 0.15 a.u. with high variation in resonance angle shift is obtained at 35:15 nm thickness of Ag and Au metals, respectively. Furthermore, Fig. 3b shows the sensitivity, detection accuracy, and figure of merit of the proposed SPR sensor for different thicknesses of Ag and Au. The values calculated for sensitivities, DAs, and FOMs are 176, 188, 197, 242, and 203 deg/RIU, 0.222, 0.163, 0.143, 0.116, and 0.107 deg^{-1}, and 39.19, 30.71, 28.18, 28.07, and 21.89 RIU^{-1}, respectively. It is obvious from Fig. 3b that the 35:15 optimized thickness ratio of Ag/Au bimetal gives high sensitivity, while DA becomes low due to the broader SPR curve. We describe the role of each of the layered used in the proposed design via the SPR curve. The SPR characteristic curves for four structures include the following: structure 1 – BK7 prism/Ag/SM, structure 2 – BK7 prism/Ag/Au/SM, structure 3 – BK7 prism/Ag/Au/WS_2(1L)/SM, and structure 4 – BK7 prism/Ag/Au/WS_2(1L)/$Ti_3C_2T_x$ MXene(1L)/SM which are presented in Fig. 4a–d, respectively. The inset graphs within Fig. 4a–d show the variation of reflection with RI of the sensing medium for 1.33 and 1.335 RIU, on the adsorption of biomolecules on the sensor surface. We calculate resonance angle shift for the sensing layer RI variation of ($\Delta n_s = 0.005$) for four structures.

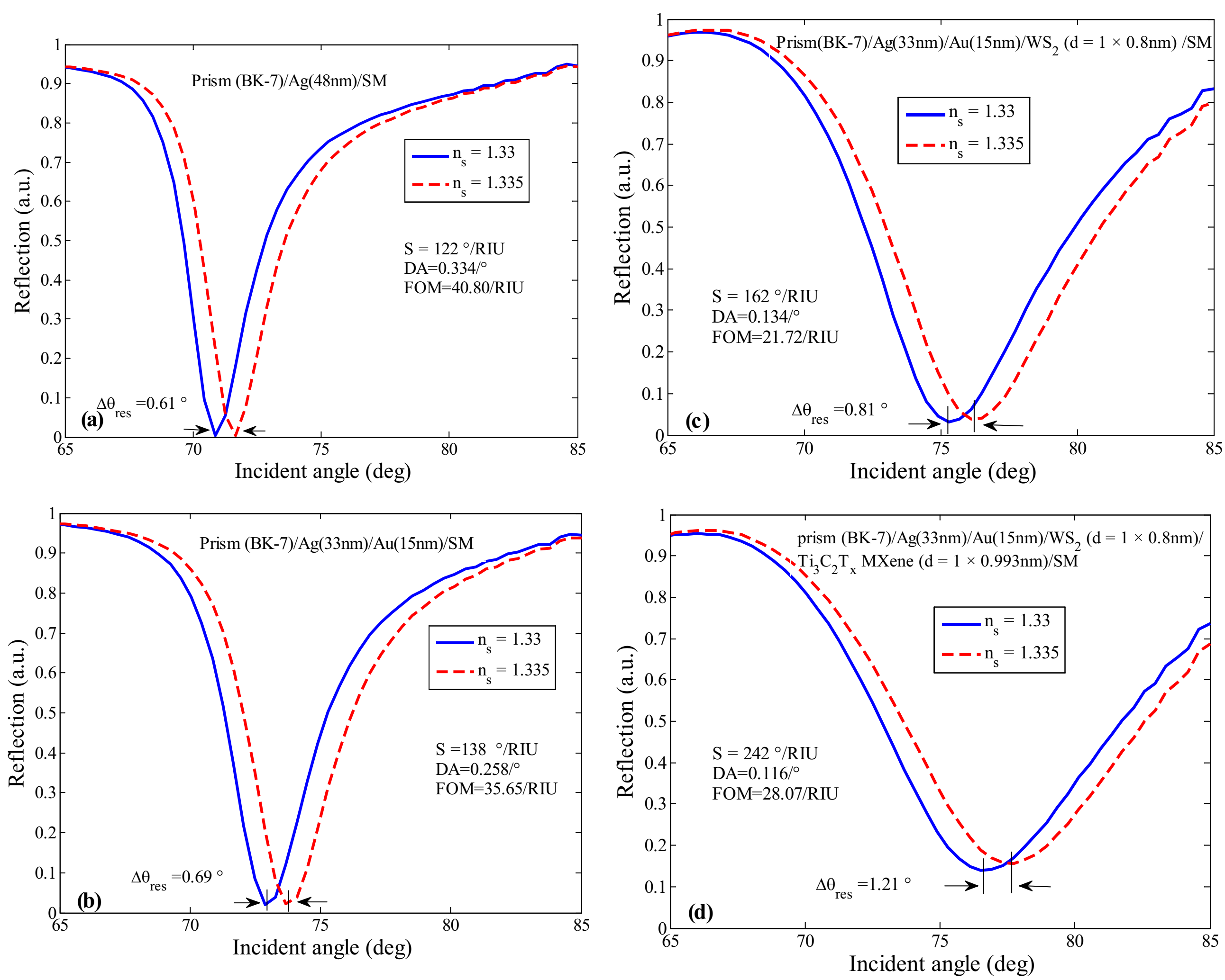

Fig. 4 The SPR curves with respect to the incident angle for **a** structure 1, **b** structure 2, **c** structure 3, and **d** the proposed SPR sensor (structure 4)

Table 1 Comparison of performance parameter between the proposed sensor with other structures

Parameters	Structures			
	Structure 1	Structure 2	Structure 3	Structure 4 (proposed)
$\Delta\theta_{res}$ (deg)	0.61	0.69	0.81	1.21
S (deg/RIU)	122	138	162	242
R_{min} (a.u.)	0.0034	0.0203	0.0312	0.1402
DA (1/deg)	0.334	0.258	0.134	0.116
FWHM (deg)	2.99	3.87	7.46	8.62
FOM (RIU^{-1})	40.80	35.65	21.72	28.07

Resonance angle shift obtained from SPR curves shown in Fig. 4a–d for structures 1, 2, 3, and 4 is 0.61, 0.69, 0.81, and 1.21 deg, respectively. Sensitivity calculated from above resonance angle shift for mentioned structures is 122, 138, 162, and 242 deg/RIU, respectively. The performance parameters FOM, DA, and FWHM calculated from SPR characteristic curves plotted in Fig. 4a–d for different SPR sensor configurations are presented in Table 1. Based on the results, it can be found that embedding the $Ti_3C_2T_x$ MXene layer in the proposed SPR sensor contributes to sensitivity enhancement. This is due to the strong charge transfer between $Ti_3C_2T_x$ MXene /WS_2 layer and bimetallic Ag/Au layers. The decrease in DA and FOM is due to lossy nature of $Ti_3C_2T_x$ MXene because of larger value of imaginary part of its refractive index. Figure 5a–d show the electric field intensity for structures 1, 2, 3, and 4. As can be seen, the strength of electric field intensity is enhanced in the proposed SPR sensor (structure 4) compared to the other structures. The layered nature of $Ti_3C_2T_x$ MXene creates a strong light-matter interaction. In fact, the use of a 2D material MXene increases the electromagnetic field within the SPs at the metal–dielectric interface. By increasing the electromagnetic field intensity, the SPP excitation in the sensing area increases and the sensitivity improves.

Figure 6 shows the absorption curve variation versus the RI of sensing layer from 1.33 to 1.35 RIU on the adsorption of biomolecules on the sensor surface. As can be seen, by increasing the RI of sensing layer, the plasmon resonance occurs at a larger angle. The performance of the sensor depends on the RI variation of the sensing medium. Changes in the RI lead to a change in the absorption curve. We have considered the SPR angle obtained for different RI values of sensing layer from $n_s = 1.33$ to 1.35 RIU for the step of 0.005 of the sensing medium.

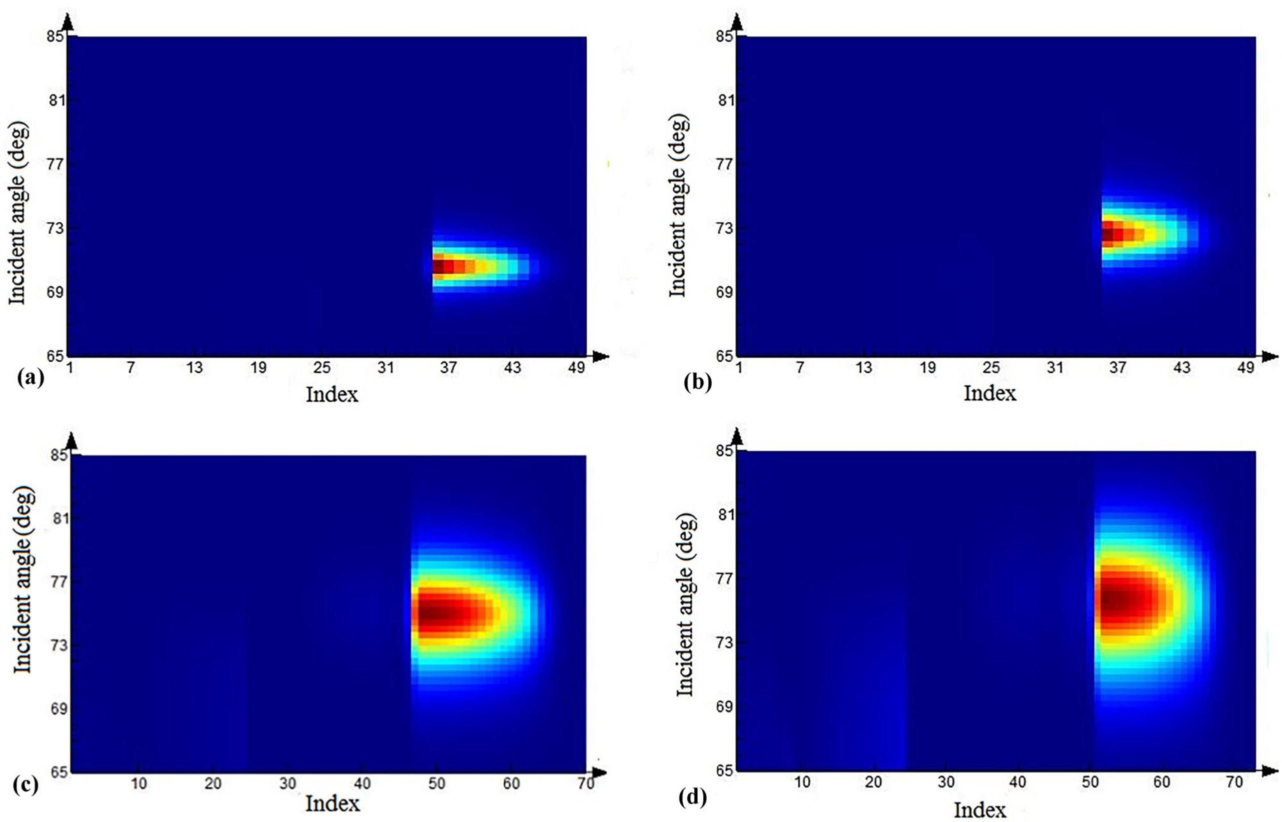

Fig. 5 Electric field intensity for **a** structure 1, **b** structure 2, **c** structure 3, and **d** the proposed SPR sensor (structure 4)

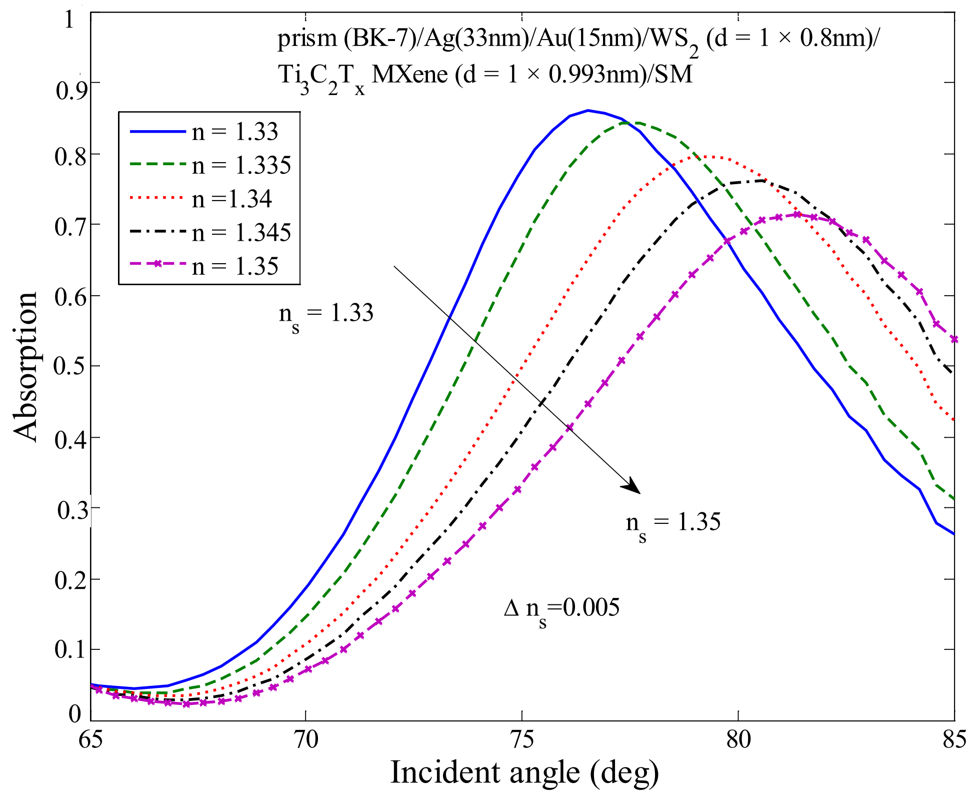

Fig. 6 The absorption curve as a function of the incident angle for different RI of sensing layer from 1.33 to 1.35 RIU for the proposed structure

Figure 7 plots the performance parameters variation with sensing layer RI for the proposed SPR sensor. The sensitivity, minimum reflection, DA, and FOM of the proposed structure varies from 242 to 287 deg/RIU, 0.1566 to 0.2854 a.u., 0.116 to 0.112 deg^{-1}, 28.07 to 32.43 RIU^{-1}, respectively, for the RI variation of sensing layer from 1.33 to 1.35 RIU. Also, to consider the effect of thickness of the $Ti_3C_2T_x$ MXene layer, we plotted the reflection curve with one layer, two layers, three layers, and four layers of $Ti_3C_2T_x$ MXene as shown in Fig. 8. The results show that when the number of the $Ti_3C_2T_x$ MXene layers increases, minimum reflection and the width of the resonance curve increase. In other

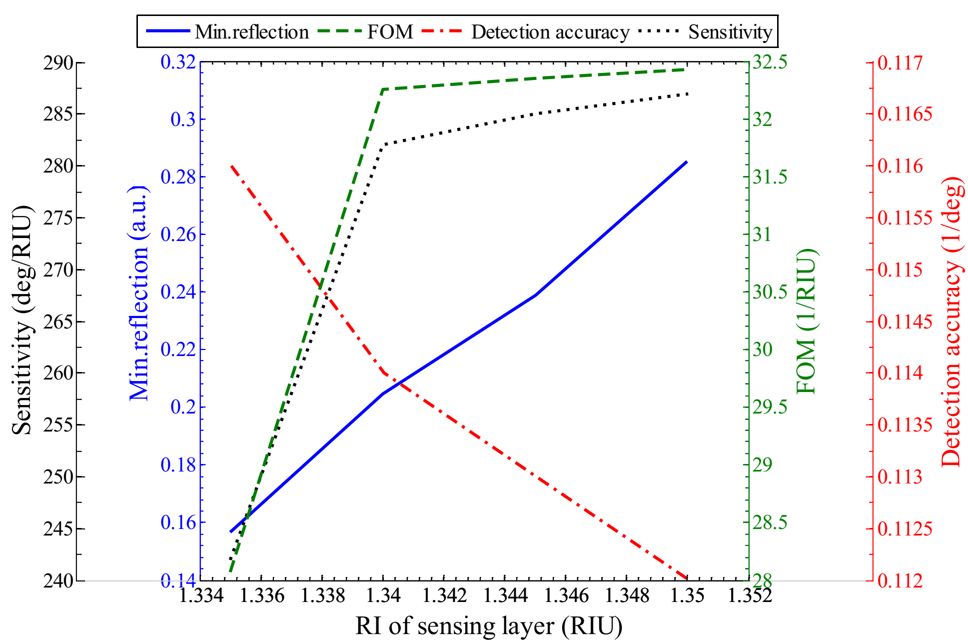

Fig. 7 Performance parameters variation vs. RI of sensing layer for the proposed SPR sensor

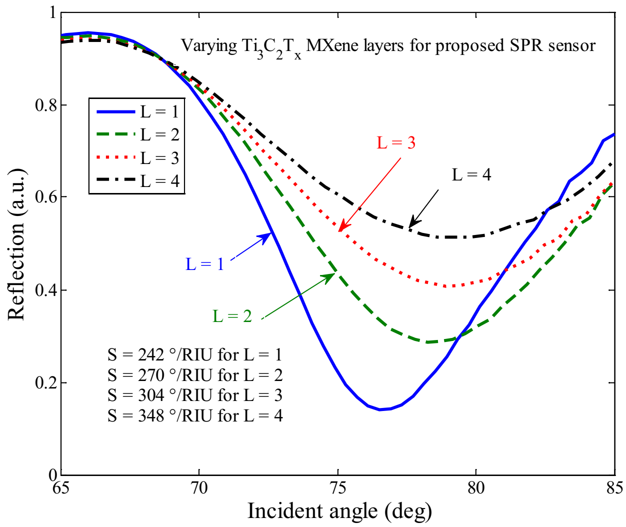

Fig. 8 The reflection curve of the proposed SPR sensor for different layers of $Ti_3C_2T_x$ MXene

words, as the number of $Ti_3C_2T_x$ MXene layers increases, the damping associated with the SPs wave increases, thereby increasing the FWHM and R_{min}.

Based on Fig. 8, the proposed SPR sensor for the case of four $Ti_3C_2T_x$ MXene layers shows maximum sensitivity of 348 deg/RIU. Sensitivity improvement is due to better confinement of charge carriers and shifts the SPR resonance angle. The interaction of the hexagonal structure of $Ti_3C_2T_x$ MXene with the analyte leads to an enhancement of the adsorption of biomolecules, and increases the sensitivity to changes in the RI, so the use of MXene improves the sensitivity of the sensor.

Absorption curves for the proposed SPR sensor are analyzed in Fig. 9a–d with different TMDs (MoS_2, $MoSe_2$, WS_2, WSe_2) layers and keeping $Ti_3C_2T_x$ MXene fixed at the monolayer. It should be noted the refractive indices of the MoS_2, $MoSe_2$, and WSe_2 are $5.0947+1.2327i$, $4.6226+1.0063i$, and $4.5502+0.4332i$, respectively, and thicknesses are 0.65, 0.70, and 0.70 nm, respectively [32–36]. Resonance angle shifts obtained from SPR curves for MoS_2, $MoSe_2$, WS_2,

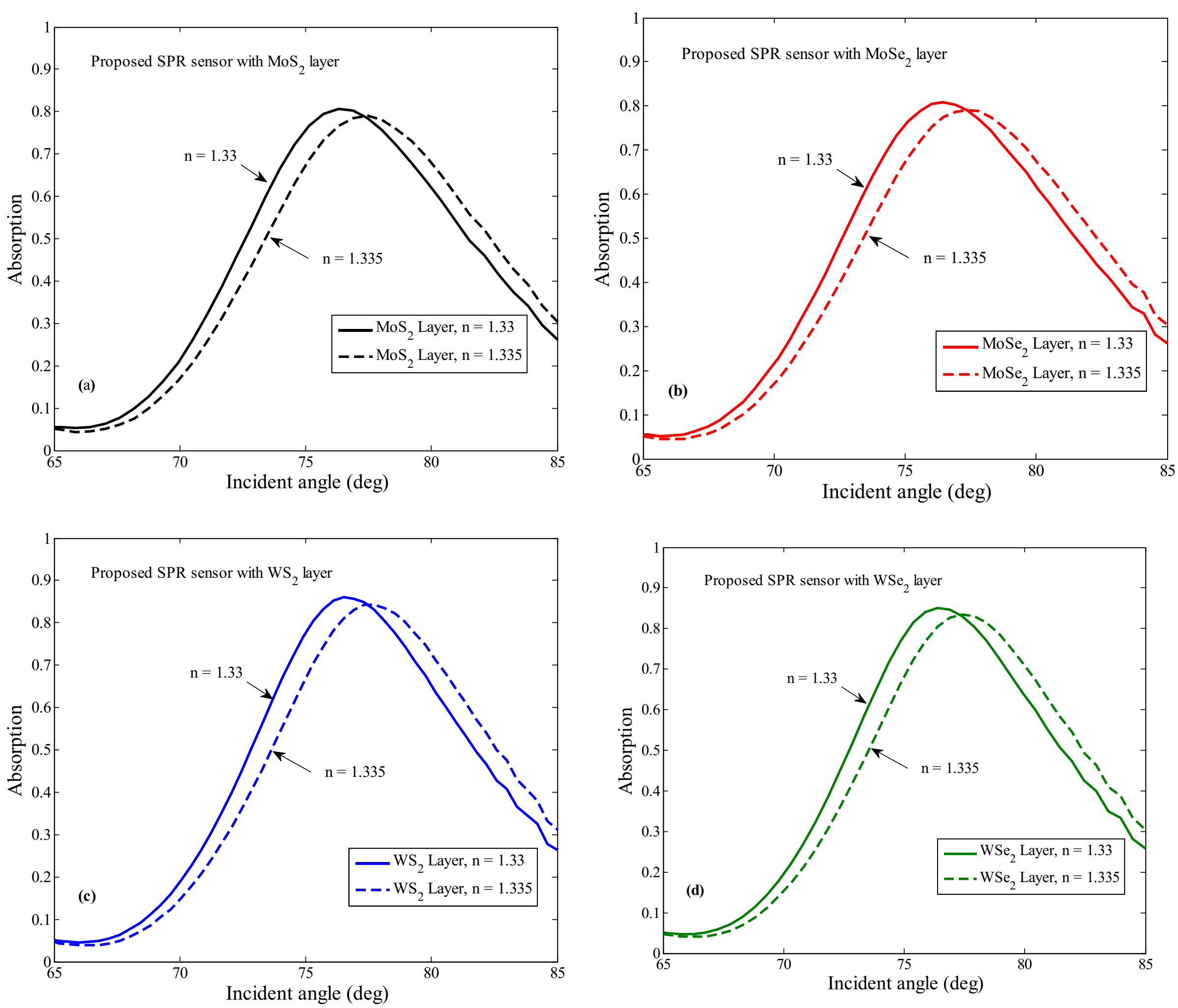

Fig. 9 Absorption curve of the proposed structure for different TMDs: **a** MoS_2 layer, **b** $MoSe_2$ layer, **c** WS_2 layer, **d** WSe_2 layer

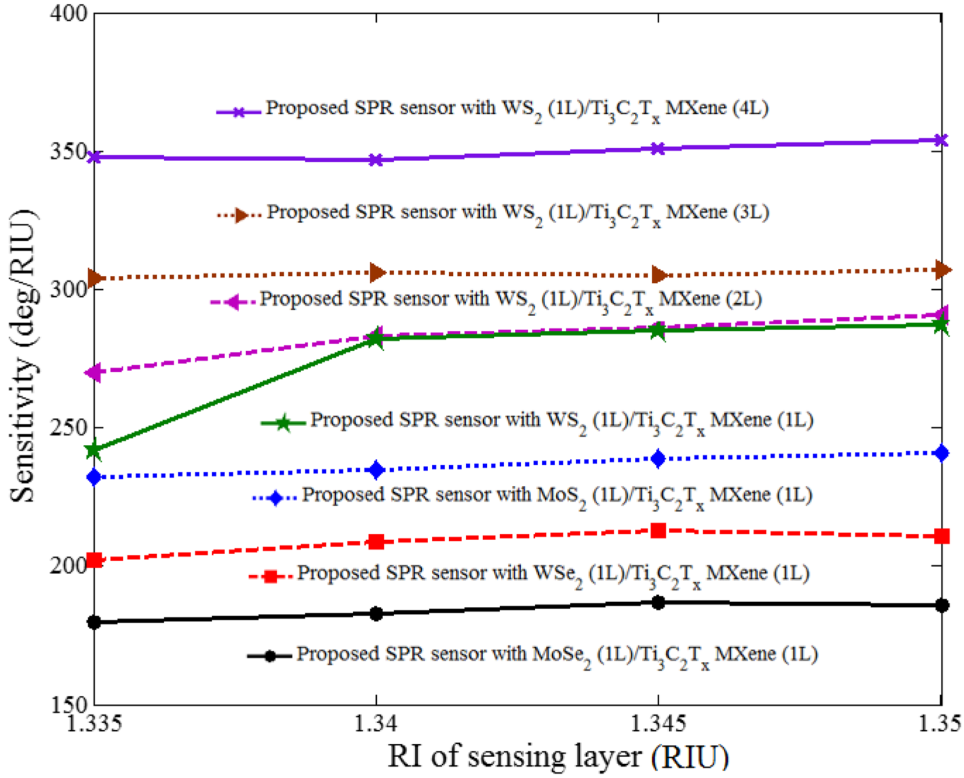

Fig. 10 Sensitivity of the proposed SPR sensor vs. the RI of the sensing layer for different TMD layers and varying layers of $Ti_3C_2T_x$ MXene

and WSe_2 are 1.16, 0.9, 1.21, and 1.01 deg, respectively. Sensitivities calculated from the above resonance angle shifts for MoS_2, $MoSe_2$, WS_2, and WSe_2 are 232, 180, 242, and 202 deg/RIU, respectively. The highest sensitivity is obtained for WS_2; this is due to the wavelength-dependent order of light absorbance of TMDs, which is least for WS_2 than WSe_2, $MoSe_2$, and MoS_2 TMD layers.

Figure 10 also shows the sensitivity variation in terms of sensing layer RI for the proposed SPR sensor with different TMDs (MoS_2, $MoSe_2$, WS_2, WSe_2) layers and varying layers of $Ti_3C_2T_x$ MXene. As can be seen, sensitivity raises with an increase in sensing layer RI for each TMDs layer. Because the light absorption capability of WSe_2, $MoSe_2$, and MoS_2 layers is higher than WS_2, the maximum sensitivity is obtained with the WS_2 layer. Also, with increasing the number of $Ti_3C_2T_x$ MXene layers from 1 to 4, the sensitivity increases. The highest sensitivity is achieved for the proposed SPR sensor with four layers of $Ti_3C_2T_x$ MXene.

Table 2 illustrates the comparison between the proposed structure with the SPR sensors explored by different research groups. The proposed SPR sensor shows the highest sensitivity compared to the other structures at 633 nm. The use of WS_2/$Ti_3C_2T_x$ MXene hybrid structure in the proposed sensor enhances the adsorption of biomolecules due to stronger Van der Waals forces, so this heterostructure improves the performance of the proposed SPR sensor. It is predicted that a novel bimetallic SPR sensor based on the 2D material $Ti_3C_2T_x$ MXene layer and WS_2 will be useful for medical diagnosis and biological applications. It is anticipated that the proposed work will be able to detect (bio)chemicals with good sensitivity and speed. Since SPR sensors have the potential to detect various types of biological and biochemical analytes. So, research on 2D materials and their heterostructures in sensing and biosensing application requires more theoretical and practical study and has the potential for further development in the coming years. We hope that the

Table 2 Comparison of the sensitivity and FOM of the proposed structure to other existing SPR sensors

Structure	Sensitivity (deg/RIU)	FOM (RIU^{-1})		Ref
BK7/Ag/Si/MXene	231	39.83	633	[30]
BK7/Al/WS_2	315.5	18.84	633	[29]
BK7/Si/MoS_2/graphene	210	-	633	[33]
BK7/Au/WSe_2/graphene	178.87	27.41	632.8	[35]
BK7/Au/BlueP-MoS_2/antimonene	194.8	25.37	633	[36]
This work	348	28.07	633	-

proposed work would educate researchers about SPR sensors and inspire them to do further research and development in this field.

Conclusion

In this work, an SPR sensor utilizing a bimetallic layer of Ag/Au with 2D material WS_2 and $Ti_3C_2T_x$ MXene based on Kretschmann configuration have studied. The different parameters of the sensor like sensitivity, DA, FOM, and FWHM had analyzed by using the FDTD method. The proposed SPR sensor has a maximum sensitivity of 242 deg/RIU with 35 nm of Ag, 15 nm of Au, a monolayer of 2D material WS_2, and one layer of $Ti_3C_2T_x$ MXene. Using four layers of $Ti_3C_2T_x$ MXene over a WS_2 layer, the highest sensitivity of 348 deg/RIU had achieved. We also investigate the function of the bimetallic layers with different TMDs (MoS_2, $MoSe_2$, WS_2, WSe_2) layers and found WS_2 layer has a better sensing performance. We expect that such promising results will lead the proposed structure as a potential candidate for detecting biomolecules and other analytes and can be used for biosensing and chemical sensing applications.

Author Contribution MG, AM, AF: software, data curation, investigation, conceptualization, methodology, writing — review and editing. AM, AF: validation, data curation, writing — original draft.

Data Availability All data included in this paper are available upon request by contact with the contact corresponding author.

Declarations

Consent for Publication All authors of this paper agree to publish our theoretical research.

Competing Interests The authors declare no competing interests.

References

1. Maier SA (2007) Plasmonics: fundamentals and applications. Springer
2. Kretschmann E, Raether H, Notizen (1965) Radiative decay of non radiative surface plasmons excited by light. Z Naturforsch A 23(12):2135–2136
3. Otto A (1968) Excitation of nonradiative surface plasma waves in silver by the method of frustrated total reflection. Z Phys 216:398–410
4. Wu L et al (2018) Few-layer $Ti_3C_2T_x$ MXene: a promising surface plasmon resonance biosensing material to enhance the sensitivity. Sens Actuators B, Chem 277:210–215
5. AlaguVibisha G et al (2020) Sensitivity enhancement of surface plasmon resonance sensor using hybrid configuration of 2D materials over bimetallic layer of Cu–Ni. Opt Commun 463(125337)
6. Raghuwanshi SK, Kumar M, Jindal SK, Kumar A, Prakash O (2020) High-sensitivity detection of hazardous chemical by special featured grating-assisted surface plasmon resonance sensor based on bimetallic layer. IEEE Trans Instrum Meas 69(7):5072–5080
7. Srivastava A, Verma A, Das R, Prajapati YK (2020) A theoretical approach to improve the performance of SPR biosensor using MXene and black phosphorus. Optik 203(163430)
8. Xu Y, Ang YS, Wu L, Ang LK (2019) High sensitivity surface plasmon resonance sensor based on two-dimensional MXene and transition metal dichalcogenide: a theoretical study. Nanomaterials 9(2):1–11
9. Rakhshani MR, Mansouri-Birjandi MA (2018) Engineering hexagonal array of nanoholes for high sensitivity biosensor and application for human blood group detection. IEEE Trans Nanotechnol 17(3):475–481
10. Ghodrati M, Mir A, Farmani A (2020) Carbon nanotube field effect transistors-based gas sensors. In: Nanosensors for Smart Cities. Amsterdam, The Netherlands: Elsevier, pp 171–183. https://doi.org/10.1016/B978-0-12-819870-4.00036-0
11. Dolatabady A, Asgari S, Granpayeh N (2018) Tunable mid-infrared nanoscale graphene-based refractive index sensor. IEEE Sensors J 18(2):569–574
12. Naderi A, Ghodrati M (2018) An efficient structure for T-CNTFETs with intrinsic-n-doped impurity distribution pattern in drain region. Turkish J Electr Eng Comput Sci 26(5):2335–2346. https://doi.org/10.3906/elk-1709-180
13. Abbasi M, Soroosh M, Namjoo E (2018) Polarization-insensitive temperature sensor based on liquid filled photonic crystal fiber. Optik 168:342–347
14. Naderi A, Ghodrati M (2017) Improving band-to-band tunneling in a tunneling carbon nanotube field effect transistor by multi-level development of impurities in the drain region. Eur Phys J Plus 132(12):510
15. Naderi A, Ghodrati M (2018) Cut off frequency variation by ambient heating in tunneling p-i-n CNTFETs. ECS J Solid State Sci Technol 7(2):M6–M10
16. Parandin F, Heidari F, Rahimi Z, Olyaee S (2021) Two-dimensional photonic crystal biosensors: a review. Opt Laser Technol 144(107397)
17. Khani S, Hayati M (2021) An ultra-high sensitive plasmonic refractive index sensor using an elliptical resonator and MIM waveguide. Superlattices Microstruct 156(106970)
18. Naderi A, Ghodrati M, Baniardalani S (2020) The use of a Gaussian doping distribution in the channel region to improve the performance of a tunneling carbon nanotube field-effect transistor. J Comput Electron 19(1):283–290
19. Ghodrati M, Farmani A, Mir A (2019) Nanoscale sensor-based tunneling carbon nanotube transistor for toxic gases detection: a first-principle study. IEEE Sensors J 19(17):7373–7377
20. Farmani A, Zarifkar A, Sheikhi MH, Miri M (2017) Design of a tunable graphene plasmonic-on-white graphene switch at infrared range. Superlattices and Microstruct 112:404–414
21. Ghodrati M, Farmani A, Mir A (2021) Non-destructive label-free biomaterials detection using tunneling carbon nanotube based biosensor. IEEE Sensors J 21(7):8847–8854
22. Vafapour Z, Troy W, Rashidi A (2021) Colon cancer detection by designing and analytical evaluation of a water-based THz metamaterial perfect absorber. IEEE Sensors J 21(17):19307–19313
23. Ghodrati M, Mir A, Naderi A (2020) New structure of tunneling carbon nanotube FET with electrical junction in part of drain region and step impurity distribution pattern. AEU-Int J Electron Commun 117(153102)
24. Ghodrati M, Mir A, Naderi A (2021) Proposal of a doping-less tunneling carbon nanotube field-effect transistor. Mater Sci Eng A: B 256(115016)
25. Mohamadi A, Seifouri M, Karami R, Olyaee S (2021) Proposal of a high-Q biosensor using a triangular photonic crystal filter. Opt Quantum Electron 53(471):1–12

26. Khozeymeh F, Razaghi M (2021) Sensitivity and intrinsic limit of detection improvement in a photonic refractive-index sensor. Optik 247(167844)
27. Hajshahvaladi L, Kaatuzian H, Danaie M (2020) A high-sensitivity refractive index biosensor based on Si nanorings coupled to plasmonic nanohole arrays for glucose detection in water solution. Opt Commun 502(127421)
28. Mozaffari MH, Ebnali-Heidari M, Abaeiani Gh, Moravvej-Farshi MK (2018) Designing a miniaturized photonic crystal based optofluidic biolaser for lab-on-a-chip biosensing applications. Org Electron 54:184–191
29. Zhao X, Huang T, Ping PS, Wu X, Huang P, Pan J, Wu Y, Cheng Z (2018) Sensitivity enhancement in surface plasmon resonance biochemical sensor based on transition metal dichalcogenides/graphene heterostructure. Sensors 18(7):2056
30. Kumar R, Pal S, Prajapati YK, Saini JP (2020) Sensitivity enhancement of MXene based SPR sensor using silicon: theoretical analysis. Silicon 13:1887–1894
31. Kumar R, Pal S, Verma A, Prajapati YK, Saini JP (2020) Effect of silicon on sensitivity of SPR biosensor using hybrid nanostructure of black phosphorus and MXene. Superlattices Microstruct 145(106591)
32. Yue C, Lang Y, Zhou X, Liu Q (2019) Sensitivity enhancement of an SPR biosensor with a graphene and blue phosphorene/transition metal dichalcogenides hybrid nanostructure. Appl Opt 58(34):9411–9420
33. Shushama KN, Rana MDM, Inum R, Hossain MDB (2017) Sensitivity enhancement of graphene coated surface plasmon resonance biosensor. Opt Quantum Electron 49(381)
34. Dong N et al (2015) Optical limiting and theoretical modelling of layered transition metal dichalcogenide nanosheets. Sci Rep 5(14646)
35. Nurrohman DT, Chiu NF (2020) Surface plasmon resonance biosensor performance analysis on 2D material based on graphene and transition metal dichalcogenides. ECS J Solid State Sci Technol 9:115023
36. Singh MK, Pal S, Prajapati YK, Saini JP (2020) Sensitivity improvement of surface plasmon resonance sensor on using BlueP/MoS2Heterostructure and antimonene. IEEE Sensors Lett 4(7):1–4